Available online at www.sciencedirect.com
ScienceDirect
Ceramics International 35 (2009) 7–12
CERAMICS INTERNATIONAL
www.elsevier.com/locate/ceramint

Processing and physical properties of Al_2O_3/aluminum alloy composites

Shang-Nan Chou [a], Horng-Hwa Lu [b], Ding-Fwu Lii [c], Jow-Lay Huang [a,*]

[a] Department of Material Science and Engineering, National Cheng-Kung University, Tainan, 701, Taiwan, ROC
[b] Department of Mechanical Engineering, National Chin-Yi University of Technology, Taiping, Taichung, 411, Taiwan, ROC
[c] Department of Electrical Engineering, Cheng Shiu Institute of Technology, Kaohsiung County, 833, Taiwan, ROC

Received 17 June 2007; received in revised form 13 July 2007; accepted 2 September 2007
Available online 25 September 2007

Abstract

Porous aluminum oxide (Al_2O_3) preforms were formed by sintering in air at 1200 °C for 2 h. A356, 6061, and 1050 aluminum alloys were infiltrated into the preforms by squeeze casting in order to fabricate Al_2O_3/A356, Al_2O_3/6061, and Al_2O_3/1050 composites, respectively, with different volumes of aluminum alloy content. The content of aluminum alloy in the composites was 10–40% by volume. The resistivity of Al_2O_3/A356, Al_2O_3/6061, and Al_2O_3/1050 composites decreased dramatically from 6.41×10^{12} to 9.77×10^{-4}, 7.28×10^{-4}, and 6.24×10^{-4} Ω m, respectively, the four-points bending strength increased from 397 to 443, 435.1, 407.2 MPa, respectively, and the deviations were smaller than 2%. From SEM microstructural analysis and TEM bright field images, the pore volume fraction and the relative density of the composites were the most important factors that affected the physical and mechanical properties. The ceramic phase and alloy phase in Al_2O_3/aluminum alloy composites were found to be homogenized and uniformly distributed using electrical and mechanical properties analysis, microstructure analysis, and image analysis.

Keywords: Al_2O_3/aluminum alloy composite; Resistivity; Four-points bending strength; Image analysis

1. Introduction

Alumina ceramic (Al_2O_3) is a hard refractory ceramic, which has been used in high temperature structural and substrate applications because of its good strength and low thermal expansion coefficient. Nevertheless, like other monolithic ceramics, Al_2O_3 is apt to suffer from low ductility and low fracture toughness. Therefore, metals (e.g. aluminum, cobalt, and niobium) or alloys are added to ceramics to improve their toughness [1–5].

Recently, the demand for lightweight materials with high strength and toughness has drawn a lot of attention to the development of ceramic-matrix composites (CMCs). CMCs represent a new class of materials, which are on their way to substituting conventional materials in many fields. In the last few years, considerable advances have been made in the development of manufacturing processes for CMCs, which have led to higher damage tolerance and a reduction in weight [6]. The biggest limitation of the fabrication of CMCs by the liquid-phase process is caused by the compatibility of the second phase and the matrix [7]. This problem is especially serious in the case of aluminum matrix composites because aluminum is usually covered with a thin oxide layer which blocks surface wetting. Several methods have been investigated to improve the compatibility at the interface [8–11]. Squeeze casting is one of the most promising processes because the contact time between the reinforcement and the aluminum melt is short [12,13].

In this study, porous Al_2O_3 preforms were formed by sintering in air at 1200 °C for 2 h. Three different aluminum alloys were chosen to be the reinforcement in composites. Molten aluminum alloys A356, 6061, and 1050 were infiltrated into the preforms by squeeze casting to make Al_2O_3/A356, Al_2O_3/6061, and Al_2O_3/1050 composites, respectively. The homogenized analysis was performed and physical and mechanical properties of the composites were measured. The effects of the composition on the homogenized analysis and physical properties were also investigated. In addition, the microstructure and uniform properties analysis of the composites were examined.

* Corresponding author. Tel.: +886 6 2348188; fax: +886 6 2763586.
E-mail address: jlh888@mail.ncku.edu.tw (J.-L. Huang).

0272-8842/$34.00
doi:10.1016/j.ceramint.2007.09.019

2. Experimental

2.1. Sample preparation

The reinforced phases used to improve strength and toughness of the Al_2O_3 ceramic matrix in this study were aluminum alloy A356, 6061, and 1050 (pure aluminum). The Al_2O_3 powders were extracted from a thermally reactive process (A16SG ALCOA, USA) with a particle size of about 0.3–0.5 μm. The structure of the Al_2O_3 powders was α phase, with a purity higher than 99.8%. The goal when selecting of three different Al alloy compositions was to choose three similar but different kinds of Al alloy. Therefore, cast treatable alloy A356, heat treatable alloy 6061, and pure aluminum 1050 were selected. In this experiment, the heat-treated state with the Al_2O_3/6061 composite was not considered because it was investigated in another experiment.

The Al_2O_3 powders were mixed homogeneously with 10, 20, 30, and 40 vol.% of paraffin wax at 80 °C. The mixture was then placed in a stainless steel die and 20 MPa of pressure was used to form the Al_2O_3 preforms. Then, the preforms were thermally debinded at 300 °C for 2 h to remove the paraffin wax and sintered in air at 1200 °C for 2 h. Porous Al_2O_3 preforms with pore contents of 10, 20, 30, and 40 vol.% were then made. The molten aluminum alloys A356 (about 690 °C), 6061 (about 740 °C), and 1050 (about 750 °C) were infiltrated into the preform to form Al_2O_3/A356, Al_2O_3/6061, and Al_2O_3/1050 composites, respectively. The squeeze casting processes included four steps: (a) preheating the casting die to 600 °C, and preparing molten A356 alloy; (b) Al_2O_3 preform setting (preheated in furnace to 600 °C); (c) high mechanical pressure for infiltration; and (d) release of pressure and extraction of the ingot [14]. During the squeeze casting process, the downward velocity of the squeeze head was 0.8–5 cm/s with a pressure of 200 MPa, and the loading time at high pressure was 30 s.

The composites were then cut and polished to 1 μm. Because of the visible difference between ceramic and aluminum alloy phases, the composites were not etched for scanning electron microscopy (SEM). The density and mechanical properties of the composites were measured, the effects of the composition on the physical and mechanical properties were investigated, and the microstructure and fracture behavior of the composite were examined.

2.2. Microstructure analysis

The phases of the as-received Al_2O_3/aluminum alloy composites were analyzed by an X-ray diffractometer (Rigaku D/Max-II BX) using Cu Kα radiation (30 kV, 20 mA) in the range of 20–90° at a speed of 4°/min. The polished specimens of the composite were examined and characterized using an optical microscope (OM). Fracture surfaces and crack propagation behavior were scrutinized using an OM and scanning electron microscopy (SEM, Hitachi S-4200) with element mapping and energy dispersive spectrometer (EDS) analysis. Etching was not necessary for optical micro-structural examination due to the adequate contrast between the bright aluminum alloy and the dark Al_2O_3.

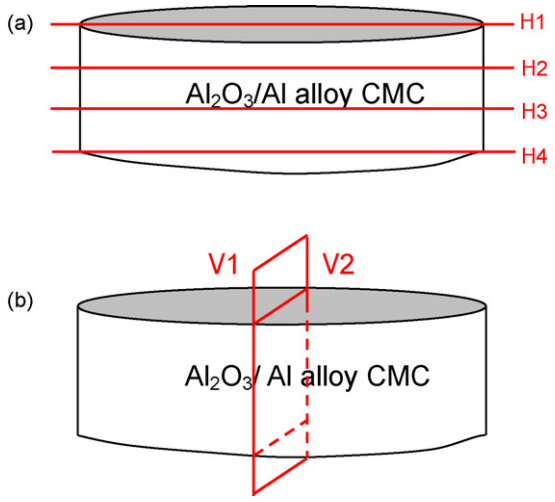

Fig. 1. A diagram of Al_2O_3/aluminum alloy composite cross section. (a) H1, H2, H3, and H4 represent the upper, two middles, and lower horizontal surfaces, respectively. (b) V1 and V2 represent the left and right vertical surfaces, respectively.

The composites were cut as diagrammed in Fig. 1. The labels H1 to H4 represent the polished horizontal surfaces, while V1 and V2 represent the polished vertical surfaces. The polished specimen surfaces of the composites were examined and characterized using an optical microscope (OM) and an image analyzer (Optimas, Vol. 1.0, imaging Fundamentals, Tacoma, WA). Each image was divided into nine discrete elements (pixels), and entered into a computer to calculate the volume fraction of the Al_2O_3/aluminum alloy composite.

2.3. Characterization of physical and mechanical properties

The density was measured using the water displacement technique. Flexural strength was measured using a four point bending test on an Instron universal testing machine (series 8511, Instron Co., Canton, MA, USA). The outer and inner spans were 40 and 20 mm, respectively. The nominal dimensions of the testing bars were $3 \times 4 \times 45\ mm^3$. The Young's modulus and Poisson's ratio were evaluated using the pulse echo method (pulse generator, model 5072, Panametrics, USA and oscilloscope, TDS540C, Tektronix, USA).

The resistance was measured by a digital multimeter (Model 182, Model 220, Model 617, Keithley Iustruments, Inc., USA) and calculated using Ohm's law, V (voltage) = I (current) × R (resistance). The resistivity was calculated using the measured resistance, electrode area, and sample thickness.

3. Results and discussion

3.1. Phase analysis

The phase analyses of the composites were performed using X-ray diffraction patterns. The results of phase analyses of

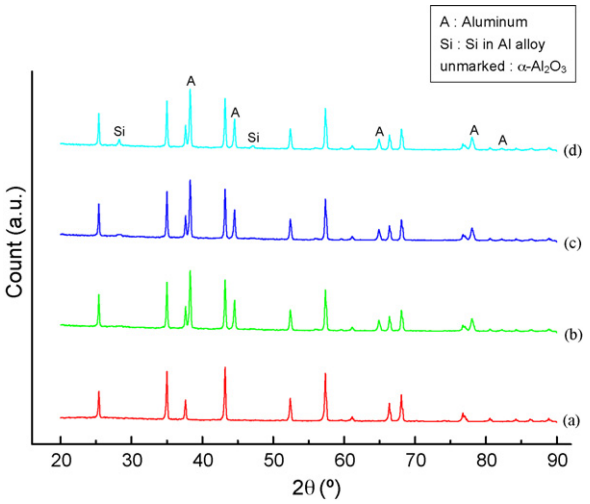

Fig. 2. X-ray diffraction patterns of (a) Al_2O_3 ceramic, (b) Al_2O_3/1050 composite, (c) Al_2O_3/6061 composite, and (d) Al_2O_3/A356 composite.

Al_2O_3 ceramic, Al_2O_3/1050 composite, Al_2O_3/6061 composite, and Al_2O_3/A356 composite are shown in Fig. 2.

Fig. 2(b), (c) and (d), respectively shows the X-ray diffraction peaks of Al_2O_3/1050, Al_2O_3/6061, and Al_2O_3/A356 composites. The composites had only α-Al_2O_3 ceramic and aluminum peaks. Only the Al_2O_3/A356 composite has a diffraction pattern peak for its 7 wt.% silicon element content. Because of the stability of α-Al_2O_3 casting with molten aluminum alloys, no other reaction product in the compositions was found [14].

Fig. 3 shows the X-ray diffraction patterns of Al_2O_3/A356 composites with H1, H2, H3, H4, V1, and V2 from Fig. 1. The composites had only α-Al_2O_3 ceramic, aluminum, and silicon element peaks. Because of the stability of α-Al_2O_3 casting with molten aluminum alloys with very short process, no other reaction product in the compositions was found. The same

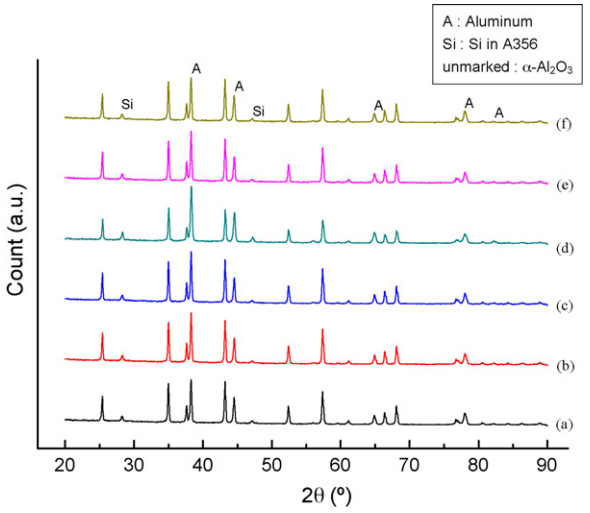

Fig. 3. X-ray diffraction patterns of Al_2O_3/A356 composite (a) upper H1 horizontal surface, (b) middle H2 horizontal surface, (c) middle H3 horizontal surface, (d) lower H4 horizontal surface, (e) left V1 vertical surface, and (f) right V2 vertical surface.

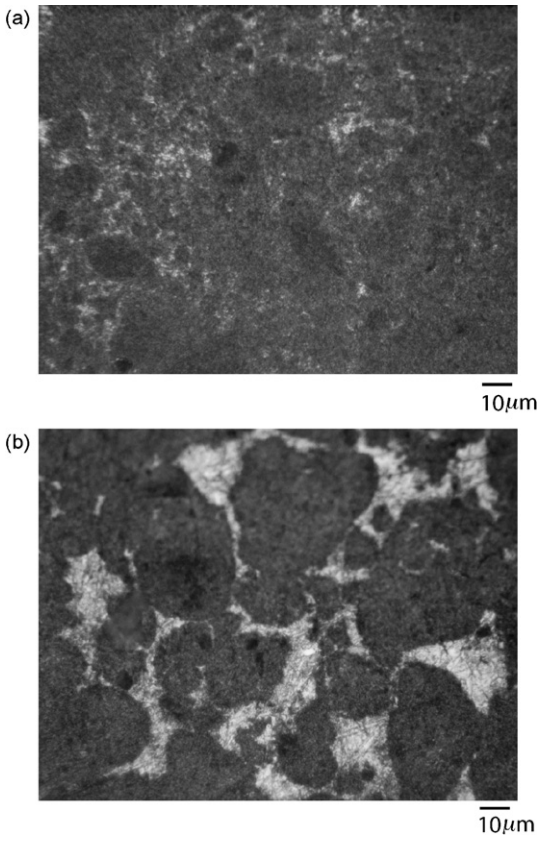

Fig. 4. Optical photographs showing the microstructure of Al_2O_3 composites with (a) 10 vol.%, and (b) 40 vol.% content A356 aluminum alloy. The bright areas are A356 alloy and the dark areas are Al_2O_3 ceramic.

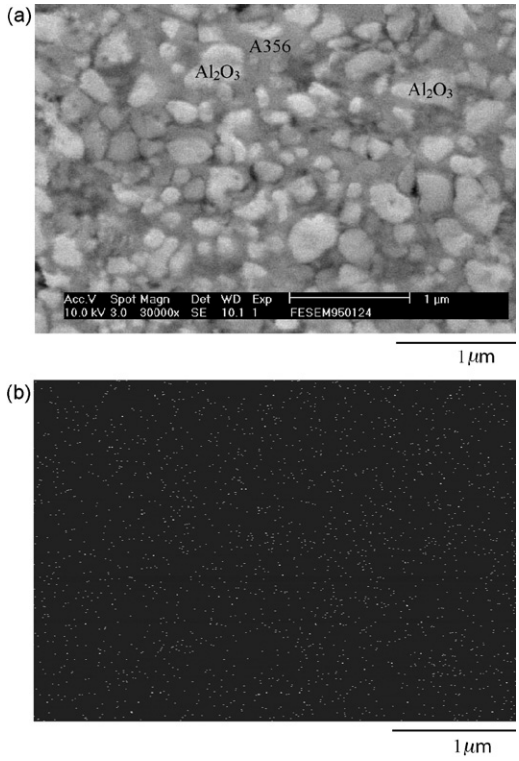

Fig. 5. (a) SEM micro-photographs showing the microstructure of the Al_2O_3/A356 composite, (b) the Si mapping process for the same area.

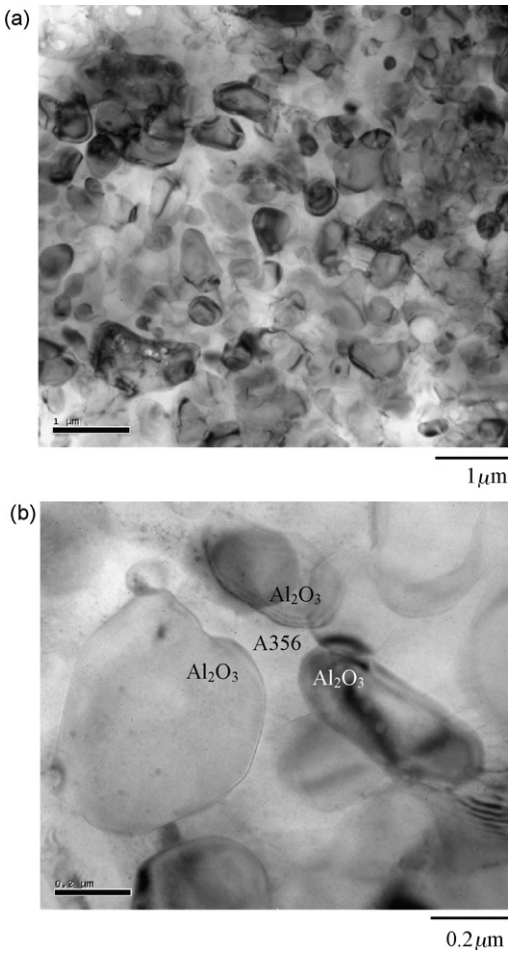

Fig. 6. TEM micro-photographs (a) showing a connected path between alumina phases. (b) The ceramic and alloy phases are closely connected.

situation was found in X-ray diffraction patterns of Al_2O_3/6061 and Al_2O_3/1050 composites.

3.2. Compositional and micro-structural analysis

All the composites were made from Al_2O_3 preforms at four aluminum alloy volume content percentages (10, 20, 30 and 40 vol.%). Typical optical photographs showing the microstructure of the Al_2O_3/A356 alloy composites are shown in Fig. 4. These two pictures show the different content volume percent in the Al_2O_3/A356 composites and the bright areas are A356 alloy and the dark areas are Al_2O_3 ceramic. The composites have a dense surface and a uniform distribution between the ceramic phase and alloy phase. The same situation was found in optical photographs of Al_2O_3/6061 and Al_2O_3/1050 composites. Typical SEM polished surface micrographs showing the microstructure of the Al_2O_3/A356 composites are shown in Fig. 5. Fig. 5(a) shows that the Al_2O_3/A356 composites with 10 vol.% A356 alloy, indicating a dense surface in the Al_2O_3/A356 composites. This is because the A356 alloy contains elementary silicon elements and has a marked fluidity and high mechanical pressure to exert upon the composites during the squeeze casting process, with the relative density of Al_2O_3/aluminum alloy composites at almost 100% [14]. Fig. 5(b) shows the silicon mapping process in the same area. The bright spots indicate the silicon elements in Fig. 5(a).

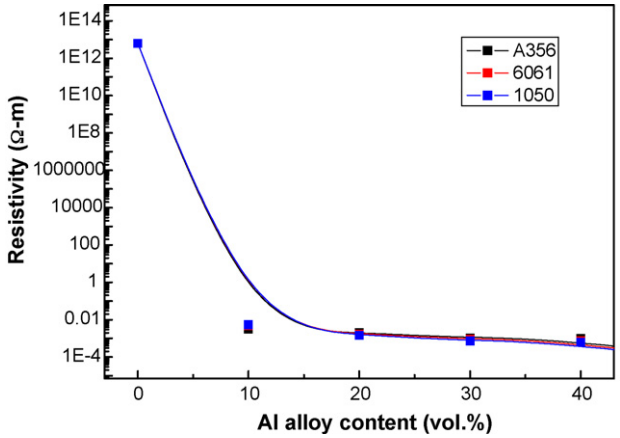

Fig. 7. Resistivity versus aluminum alloy content in the Al_2O_3/aluminum alloy composites.

Table 1
The SEM micro-photograph image analyzer results about alloy volume fractions by percentages (%) of (a) A356 aluminum alloy, (b) 6061 aluminum alloy, and (c) 1050 aluminum alloy in Al_2O_3/aluminum alloy composites

(a)	A10	A20	A30	A40
H1	9.9 ± 0.2	19.8 ± 0.3	29.8 ± 0.2	39.7 ± 0.2
H2	10.2 ± 0.2	20.1 ± 0.3	30.1 ± 0.3	40.3 ± 0.1
H3	10.3 ± 0.2	20.3 ± 0.4	30.2 ± 0.4	40.3 ± 0.3
H4	10.1 ± 0.1	19.9 ± 0.1	30.0 ± 0.1	39.8 ± 0.1
V1	10.3 ± 0.1	20.2 ± 0.2	30.3 ± 0.3	40.5 ± 0.2
V2	9.8 ± 0.3	19.9 ± 0.2	29.9 ± 0.2	39.7 ± 0.3
Average	10.1 ± 0.15	20.0 ± 0.25	30.2 ± 0.2	40.0 ± 0.2
(b)	A10	A20	A30	A40
H1	10.1 ± 0.3	20.4 ± 0.2	30.2 ± 0.1	40.1 ± 0.1
H2	10.3 ± 0.1	20.2 ± 0.1	30.2 ± 0.3	40.2 ± 0.3
H3	10.1 ± 0.2	20.4 ± 0.3	30.1 ± 0.2	40.4 ± 0.2
H4	10.2 ± 0.2	19.9 ± 0.2	30.3 ± 0.2	40.2 ± 0.2
V1	10.4 ± 0.4	20.1 ± 0.3	30.4 ± 0.1	39.9 ± 0.3
V2	9.9 ± 0.1	20.3 ± 0.1	30.1 ± 0.4	40.5 ± 0.1
Average	10.2 ± 0.22	20.2 ± 0.2	30.2 ± 0.22	40.2 ± 0.2
(c)	A10	A20	A30	A40
H1	10.3 ± 0.4	20.2 ± 0.3	29.7 ± 0.3	40.3 ± 0.1
H2	10.1 ± 0.1	20.4 ± 0.4	30.3 ± 0.1	39.8 ± 0.4
H3	10.4 ± 0.3	20.2 ± 0.1	30.4 ± 0.2	40.1 ± 0.2
H4	10.2 ± 0.2	20.1 ± 0.3	30.2 ± 0.2	40.2 ± 0.3
V1	10.1 ± 0.3	20.4 ± 0.2	30.1 ± 0.4	40.4 ± 0.4
V2	10.0 ± 0.2	19.7 ± 0.1	30.3 ± 0.1	40.3 ± 0.2
Average	10.2 ± 0.25	20.2 ± 0.23	30.2 ± 0.22	40.2 ± 0.27

Table 2
The physical properties of the aluminum alloys

Aluminum alloy	Density (g/cm^3)	Resistivity (Ω m)	Melting point (°C)
A356	2.71	4.21×10^{-8}	560–580
6061	2.70	3.97×10^{-8}	580–650
1050	2.705	2.61×10^{-8}	660

Table 3
Four-point bending strengths and deviation versus aluminum alloy content in the Al_2O_3/aluminum alloy composites

Alloy content (wt.%)	Al alloy					
	A356		6061		1050	
	Strength (MPa)	Deviation (%)	Strength (MPa)	Deviation (%)	Strength (MPa)	Deviation (%)
0	397	1.66	397	1.66	397	1.66
10	482.5	1.68	463.3	1.94	384.8	3.64
20	463.8	1.55	447.7	1.85	418.7	2.20
30	457	1.62	441.2	1.72	412.4	2.01
40	443	1.53	435.1	1.65	407.2	1.79

The distribution of silicon elements is uniform and homogenized. This means that the second phase of the composites is also uniform and homogenized. Typical TEM bright field images showing the microstructure of the Al_2O_3/A356 composites are shown in Fig. 6. Fig. 6(a) shows that the Al_2O_3/A356 composite has a uniform distribution between and the ceramic phase and alloy phase. Fig. 6(b) shows that the ceramic phase and alloy phase are closely connected in the Al_2O_3/A356 composite. The same situation is also true for optical photographs of Al_2O_3/6061 and Al_2O_3/1050 composites.

The composites were examined and characterized using an optical microscope and an image analyzer by Optimas. Table 1 shows the image analyzer results about alloy volume fractions by percentages (%) of Al_2O_3/aluminum alloy composites cut as in Fig. 1. Each image was divided into nine discrete elements, and entered into a computer to calculate the volume fraction of Al_2O_3/aluminum alloy composite. The ceramic phase and alloy phase in Al_2O_3/aluminum alloy composites are homogenized and uniformly distributed on all surfaces of the composites.

3.3. Physical and mechanical properties

3.3.1. Electrical property

The results of electrical property measurements are shown in Fig. 7. The resistivity decreased dramatically from 6.41×10^{12} to 9.77×10^{-4}, 7.28×10^{-4}, and $6.24 \times 10^{-4}\ \Omega$ m with Al_2O_3/A356, Al_2O_3/6061 and Al_2O_3/1050 composites, respectively, by adding aluminum alloy content in the composites from 0 to 40 vol.%. In previous research, the correlation existing between electrical conductivity and connectivity of the alloy phase was affect the electrical conductivity of the composites, and the resistivity decreased dramatically with minimum deviations when the conductor reinforcement alloy phase in the composites was homogenized and uniformly distributed [15]. As shown in Fig. 7, the composites with the three kinds of alloys are homogenized and uniformly distributed because the aluminum alloy is a completely conductible material. The resistivity of pure aluminum alloy is shown in Table 2. The resistivity of CMCs decreases with increasing aluminum alloy contents from 0 to 40 vol.%, and the three curves are very similar. Obviously, electrical conductivity almost does not change when moving from 10 to 40 vol.% of metal. This suggests that the connectivity of the alloy phase of the composite already exists for the lowest (10 vol.%) alloy content composite, and one can observe the connectivity of the alloy phase of the composite in Fig. 4. Therefore, all the electrical conductivities of the composites were almost the same, that was due to the alloy phase of the composite were all connective. The resistivity of the composites was similar. The differences in Al_2O_3/aluminum alloy composites with 40 vol.% aluminum alloy for aluminum alloys A356, 6061, and 1050 are shown in Table 2. Therefore, the basic alloy phases control the electrical properties of the composites.

3.3.2. Mechanical properties

Table 3 shows the four-points bending strengths and the deviation relating to different aluminum alloy content of the Al_2O_3/aluminum alloy composites. The four-points bending strength of the composites increased from 397 to 482.5 MPa, and from 397 to 463.3 MPa after increasing the A356 and 6061 alloy contents, respectively, from 0 to 10 vol.%. The strength decreased from 482.5 to 443 MPa, and from 463.3 to 435.1 MPa after further increasing the A356 and 6061 alloy content, respectively, from 10 to 40 vol.%. This occurred because the relative density increased from 97.5 to about 100%. Although the strength decreases with A356 content increasing from 10 to 40 vol.%, the relative densities were the same at about 100%. The strength decreases because the materials were infiltrated with the soft material aluminum alloy [16]. The same phenomenon was found for the Al_2O_3/1050 composite bending strength, which increased from 384.8 to 418.7 MPa with 1050 alloy content increasing from 10 to 20 vol.%. This occurred because the relative density was about 100%.

In addition, all the diffractions are smaller than 2%, except the diffraction for the Al_2O_3/1050 composite with 10 vol.% aluminum alloy, which was slightly greater than 3%. There are several cavities and holes in Al_2O_3/1050 composites with 10 vol.% aluminum alloy [17], and these cavities and holes effect make greater diffractions.

4. Conclusion

The resistivity decreased dramatically from 6.41×10^{12} to 9.77×10^{-4}, 7.28×10^{-4}, and $6.24 \times 10^{-4}\ \Omega$ m with Al_2O_3/A356, Al_2O_3/6061 and Al_2O_3/1050 composites, respectively, by adding aluminum alloy from 10 to 40 vol.%. The deviations were smaller than 2%, except for the deviation in the Al_2O_3/1050 composite with 10 vol.% aluminum alloy, which was greater than 3%. The ceramic phase and alloy phase in Al_2O_3/

aluminum alloy composites are homogenized and uniformly distributed.

Acknowledgment

The authors would like to thank National Science Council of the Republic of China for its financial support under Contract No. NSC-95-2623-7-006-008-D.

References

[1] C. Toy, W.D. Scott, Ceramic–metal composite produced by melt infiltration, J. Am. Ceram. Soc. 73 (1) (1990) 97–101.
[2] B.D. Flinn, M. Ruhle, A.G. Evans, Toughening in composites of reinforced with Al, Acta Metall. 37 (11) (1989) 3001–3006.
[3] D.C. Halverson, A.J. Pyzik, I.A. Aksay, W.E. Snowden, Processing of boron carbide/aluminum composites, J. Am. Ceram. Soc. 72 (5) (1988) 775–780.
[4] L.S. Sigl, H.F. Fischmeister, On the fracture toughness of cemented carbides, Acta Metall. 36 (4) (1988) 887–897.
[5] L. Shaw, R. Abbaschian, Toughening $MoSi_2$ with niobium metal—effects of morphology of ductile reinforcement, J. Mater. Sci. 30 (1995) 849–854.
[6] A.G. Evans, R. Naslain (Eds.), High-temperature ceramic-matrix composites. II. Manufacturing and materials development. Ceramic Transaction, vol. 58, The American Ceramic Society, 1995.
[7] A. Alonso, A. Pamies, J. Narciso, C. Garciacordovilla, E. Louis, Metal. Trans. 24A (6) (1993) 1423–1432.
[8] R. Smith, F.H. Fores, J. Metal. (1992) 85.
[9] S.-W. Lai, D.D.L. Chung, Fabrication of particle aluminium–matrix composites by liquid metal infiltration, J. Mater. Sci. 29 (1994) 3128–3150.
[10] P.K. Rohtagi, D. Nath, S.S. Singh, B.N. Keshavaram, J. Mater. Sci. 129 (1994) 5970.
[11] A.-B. Ma, H. Gan, T. Imura, Y. Nishida, J.Q. Jiang, M. Takagi, Wear properties of aluminum alloy reinforced by short alumina fibers with gradient distribution, Mater. Trans. 38 (9) (1997) 812–816.
[12] S. Chu, R. Wu, Compos. Sci. Technol. 59 (1999) 157–162.
[13] A.M. Assar, M.A. Al-Nimir, J. Compos. Mater. 28 (1994) 1480.
[14] D.-F. Lii, J.-L. Huang, S.-T. Chang, J. Eur. Ceram. Soc. 22 (2002) 253–261.
[15] W.H. Tuan, M.C. Lin, H.H. Wu, Preparation of Al_2O_3/Ni composites by pressureless sintering in H_2, Ceram. Int. 21 (4) (1995) 221–225.
[16] S.N. Chou, J.L. Huang, D.F. Lii, H.H. Lu, The mechanical properties of Al_2O_3/aluminum alloy A356 composite manufactured by squeeze casting, J. Alloys Compd. 419 (1–2) (2006) 98–102.
[17] S.N. Chou, J.L. Huang, D.F. Lii, H.H. Lu, The mechanical properties and microstructure of Al_2O_3/aluminum alloy composites fabricated by squeeze casting'', J. Alloys Compd. 436 (1–2) (2007) 124–130.